Long-period tidal variations in the length of day

Citation	Ray, R. D., and S. Y. Erofeeva (2014), Long-period tidal variations in the length of day, Journal of Geophysical Research: Solid Earth, 119, 1498–1509. doi:10.1002/2013JB010830
DOI	10.1002/2013JB010830
Publisher	American Geophysical Union
Version	Version of Record
Terms of Use	http://cdss.library.oregonstate.edu/sa-termsofuse

AGU PUBLICATIONS

JGR

Journal of Geophysical Research: Solid Earth

RESEARCH ARTICLE

10.1002/2013JB010830

Key Points:
- A new model of LOD tidal oscillations with periods 1 week to 18.6 years
- Dynamic ocean and anelastic mantle effects included for all constituents
- The model largely eliminates tidal variance in observed Earth rotation data

Correspondence to:
R. D. Ray,
richard.ray@nasa.gov

Citation:
Ray, R. D., and S. Y. Erofeeva (2014), Long-period tidal variations in the length of day, *J. Geophys. Res. Solid Earth*, *119*, 1498–1509, doi:10.1002/2013JB010830.

Received 6 NOV 2013
Accepted 27 JAN 2014
Accepted article online 4 FEB 2014
Published online 27 FEB 2014

Long-period tidal variations in the length of day

Richard D. Ray[1] and Svetlana Y. Erofeeva[2]

[1]NASA Goddard Space Flight Center, Greenbelt, Maryland, USA, [2]College of Earth, Ocean, & Atmospheric Sciences, Oregon State University, Corvallis, Oregon, USA

Abstract A new model of long-period tidal variations in length of day is developed. The model comprises 80 spectral lines with periods between 18.6 years and 4.7 days, and it consistently includes effects of mantle anelasticity and dynamic ocean tides for all lines. The anelastic properties follow Wahr and Bergen; experimental confirmation for their results now exists at the fortnightly period, but there remains uncertainty when extrapolating to the longest periods. The ocean modeling builds on recent work with the fortnightly constituent, which suggests that oceanic tidal angular momentum can be reliably predicted at these periods without data assimilation. This is a critical property when modeling most long-period tides, for which little observational data exist. Dynamic ocean effects are quite pronounced at shortest periods as out-of-phase rotation components become nearly as large as in-phase components. The model is tested against a 20 year time series of space geodetic measurements of length of day. The current international standard model is shown to leave significant residual tidal energy, and the new model is found to mostly eliminate that energy, with especially large variance reduction for constituents Sa, Ssa, Mf, and Mt.

1. Introduction

The Earth's rotation rate, and thus the length of day (LOD), varies on all time scales from a multitude of causes. One of the largest variations is induced by the long-period zonal body tides, which in essence act to modulate the Earth's flattening and thereby its moment of inertia. These tides range in period from 18.6 years to 5 days; at periods between a week and a month, and especially near one fortnight, they dominate all other effects in LOD [*Lambeck*, 1980].

Accurate models of these long-period tidal variations are needed for many purposes. For more than 30 years the geodetic community has relied heavily on a fundamental paper by *Yoder et al.* [1981], who presented a model based on an elastic mantle decoupled from the core and an ocean tide in equilibrium with the astronomical potential. Their work has undergone various adaptations from time to time to adjust constants or to improve secondary effects such as dynamic ocean contributions. The current standard model, adopted as part of the 2010 Conventions of the International Earth Rotation and Reference Systems Service (IERS), continues to rely on the Yoder et al. work, but modified as follows: of the 62 spectral lines in the original table, four constituents (comprising five lines) were adjusted for effects of mantle anelasticity and two constituents were adjusted for effects of dynamic ocean tides [*Petit and Luzum*, 2010, Chapter 8]. *Gross* [2009] discusses the model in some detail and compares the oceanic terms with those of several other published tide models.

Our goal here is twofold: (1) to develop a new model, one more complete and consistent in the sense that anelastic and dynamic oceanic effects are included in all spectral lines of the long-period band and (2) to improve the accuracy of the model. The immediate impetus is to build on recent work with the near-fortnightly Mf constituent [*Ray and Egbert*, 2012]. That work presented experimental confirmation of a 30 year old theoretical model of mantle anelasticity by *Wahr and Bergen* [1986], and it therefore suggests the Wahr-Bergen model is an appropriate candidate for incorporating anelastic effects throughout the long-period band. A second result of our Mf work was the finding that purely numerical ocean models of the Mf tide can be developed which are, at least for LOD predictions, very nearly as accurate as models that assimilate data (e.g., tide gauge or satellite altimetry). This is extremely relevant for any work that aims to develop models for other long-period constituents, since only Mf (and perhaps Mm and Mt) is large enough to be measured with much fidelity in ocean data. For all other constituents we must rely on numerical ocean models that do not assimilate data and hope that our experience with Mf holds when extended to these other frequencies. LOD measurements themselves may well provide the best test of this approach.

In section 2 we revisit the tidal frequencies to be included in the model. Section 3 is then devoted to the development of the body tide LOD model, and section 4 to the ocean tide model. Section 5 tests the model against space-geodetic measurements of LOD.

Tidal perturbations in rotation rate may be variously described in terms of excess length of day $\Delta\Lambda$, variations in Universal Time ΔUT1 relative to international atomic time TAI, or as a generalized response coefficient κ [*Agnew and Farrell*, 1978]. The first two are related by

$$\Delta\mathrm{UT} = -\Lambda_0^{-1}\int \Delta\Lambda \, dt$$

where Λ_0 is the nominal length of day (86,400 s). Taking now a general tidal variation of frequency ω and converting to complex notation, we have the following relationships between the three LOD variables:

$$\Delta\mathrm{UT} = i(\omega\Lambda_0)^{-1}\Delta\Lambda$$

and

$$\Delta\Lambda = \kappa^*\Lambda_0\frac{R^3}{3GC}\left(\frac{5}{\pi}\right)^{1/2}V_0$$

where R is the mean Earth radius, G the Newtonian constant, C the polar moment of inertia, and V_0 is the potential amplitude with normalization (following Agnew and Farrell) as in *Munk and Cartwright* [1966] and *Cartwright and Tayler* [1971]. More specifically, the long-period potential at the Earth's surface is written

$$\Phi(\theta, t) = \sqrt{(5/16\pi)}\,(1 - 3\cos^2\theta)\,V_0\cos(\omega t) \quad (1)$$

where θ is colatitude. For example, for the Mf constituent V_0 is 0.65258 $m^2\ s^{-2}$.

Beginning in section 3 the various geophysical components of the LOD model are constructed. It will be helpful to express the admittance κ as composed of three parts: an elastic body tide, a much smaller anelastic body tide perturbation, and an ocean tide:

$$\kappa = \kappa_e + \kappa_a + \kappa_o.$$

The ocean admittance includes a small part arising from effects of the load tide.

2. Tidal Catalog

It is worth revisiting the tidal potential expansion adopted by *Yoder et al.* [1981], since it appears that some neglected small terms are probably now detectable, or nearly so. For their tidal expansion Yoder et al. used a selection of the terms developed in the nutation theory of *Kinoshita* [1977], much as *Woolard* [1959] had previously used his own earlier nutation theory [*Woolard*, 1953]. Woolard acknowledged he could have used the existing (and more complete) expansion of the tidal potential by *Doodson* [1921]. In fact, that is the approach we prefer, although obviously with a more modern, expanded development. We here begin with the tidal catalog of *Hartmann and Wenzel* [1995], which comprises 12,935 spectral lines, including 1483 from direct attraction by planets Mercury through Saturn.

The 62 long-period terms adopted by *Yoder et al.* [1981] included all lines whose effect on ΔUT exceeds 2 μs. UT1, being an integration of the tidal perturbations over time, tends to emphasize longer-period tides. There are, however, a number of shorter period lines in $\Delta\Lambda$ that Yoder et al. neglected but which modern space-geodetic measurements are probably capable of detecting. Therefore, in addition to the Yoder threshold of 2 μs in UT, we also include lines that exceed 0.4 μs in LOD. This brings in an additional 17 lines, one with period 15.906 days and all the others at periods 12.787 days or shorter. The shortest period term is now at 4.684 days, whereas for Yoder et al. it was 5.638 days. None of the planetary lines in the Hartmann-Wenzel table is large enough to pass either thresholds, so all lines here are either lunar and/or solar, as usual.

One additional small line, for a total of 80, occurs at the very lowest frequency in our table, differing from the argument of the 18.6 year node tide by $-2p_s$ where p_s is the mean longitude of solar perihelion. Couplets of lines differing by $\pm 2p_s$ can be seen throughout the Hartmann-Wenzel tables, even for the semidiurnal M_2 constituent, and it is evidently not uncommon in potential expansions based on numerical harmonic analysis (as opposed to algebraic analysis, although a couplet in Sa occurs in all catalogs, even Doodson's); see in

particular discussions on this matter by *Roosbeek* [1996] and *Kudryavtsev* [2004]. The latter author routinely combines such couplets, but at the expense of nonzero out-of-phase components, which Hartmann and Wenzel avoid. The new line here is practically negligible in comparison with the main nodal line, but it does rise above the 2 μs cutoff, so we shall retain it.

One final point about the tidal potential concerns possible secular trends. In an earlier computation of the tide-generating potential at three epochs separated by about 50 years, *Cartwright and Tayler* [1971] noticed that several lines are undergoing discernible secular trends. *Hartmann and Wenzel* [1995] explicitly account for this by computing linear rates for all spectral lines in their potential. *Kudryavtsev* [2004] also includes quadratic terms. In the long-period band of interest here, the most significant trends are in Ssa and Mf, both of which are declinational tides and so are presumably responding to the present-day decrease in obliquity of about 47″ per century. The trend in Mf is approximately −0.1% per century, which in light of our other thresholds we can here ignore. So our model corresponds to the epoch of the constant terms in the Hartmann-Wenzel tables, which is J2000. As the space-geodetic time series continues to lengthen, this time dependence must eventually be revisited.

3. Body Tides

For the elastic body tide contribution we adopt a frequency-independent admittance computed by *Benjamin et al.* [2006]. Their computation follows exactly the earlier work of *Wahr et al.* [1981] but employs the preliminary reference Earth model (PREM) rather than the older 1066A model used by Wahr et al. The LOD admittance κ_e is found to be 0.2639. For the fortnightly Mf potential, this PREM-based admittance corresponds to a ΔUT amplitude of 656 μs. *Wahr et al.* [1981] gave 663 μs for 1066A; *Defraigne and Smits* [1999] computed 654 μs for PREM, close to the Benjamin et al. value.

As noted in section 1, for the anelastic part of the body tide we adopt the frequency-dependent model of *Wahr and Bergen* [1986]. In that work results were presented for two different anelastic models. The Wahr-Bergen "Model B" is marginally closer to our empirical estimate for the fortnightly constituent [*Ray and Egbert*, 2012], so we here adopt that model. Ultimately, based on earlier work by *Sipkin and Jordan* [1980] and *Smith and Dahlen* [1981], Model B provides a very simple two-shell description of shear dissipation in the mantle, with an upper mantle Q of 108 and a lower mantle Q of 225, both representing gross averages over a seismic frequency band of 6–60 mHz. *Smith and Dahlen* [1981] extrapolated these Q values to lower frequencies by exploiting the probable linearity in strain [*Agnew*, 1981] and assuming a single absorption band with frequency dependence

$$Q(\omega) = (\omega/\omega_m)^{\alpha}\, Q(\omega_m) \tag{2}$$

for some reference frequency ω_m in the seismic band and $-1 \le \alpha \le 1$. From an analysis of the Chandler wobble, Smith and Dahlen determined $\alpha = 0.09$ for Model B with $\omega_m = 2\pi/(30\,\mathrm{s})$.

Probably the greatest uncertainty in our LOD model and the potential source of the largest error involves extrapolation of these anelastic effects to the very long periods of the lunar node tide at 18.6 years. The value $\alpha = 0.09$ [*Smith and Dahlen*, 1981] is somewhat smaller than is generally nowadays employed [e.g., *Mathews et al.*, 1997]. The exact value is not especially critical at lower frequencies around Mf, but after extrapolation to 18.6 y it would be. Unfortunately, there are no truly reliable observational constraints at those long periods. Some of the most valuable data come from laser tracking of the LAGEOS satellites [e.g. *Lambeck and Nakiboglu*, 1983], which has now reached a time span of two nodal cycles, yet the interpretation of those data is becoming more and more problematic, quite possibly because of recently increasing polar ice melt [e.g., *Cheng et al.*, 2013]. LAGEOS tracking analyses were used by *Benjamin et al.* [2006]; their results are consistent with a range of α values and do not rule out 0.09; see their Figure 7, which was computed for a reference period of 200 s (a reference period of 30 s, as we are using, moderately improves the consistency with a low value for α). In summary, while our extrapolation to 18.6 years is a likely source of error, the lack of useful constraints suggests that adopting the Wahr-Bergen model consistently throughout the entire long-period tidal band is the simplest, most straightforward approach and cannot be ruled out on the basis of current evidence.

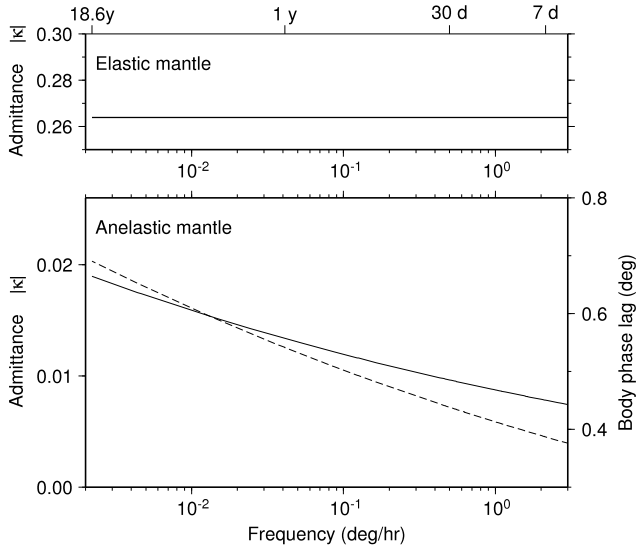

Figure 1. (top) LOD admittance κ_e for the elastic part of the body tide, which does not vary with frequency. The value is 0.26386. (bottom) Admittance κ_a for the anelastic part, based on Model B of *Wahr and Bergen* [1986] (solid line). Dashed curve is the phase lag for the total body tide effect in LOD, i.e., $-\arg(\kappa_e + \kappa_a)$, roughly 0.5°, but slowly increasing with tidal period.

Combining equations of *Wahr and Bergen* [1986, equations (5.16) and (6.2)], we find the contribution of the anelastic mantle to the LOD admittance can be expressed as

$$\kappa_a(\omega) = \left\{-0.0344\, R(\omega, Q_a) - 0.569\, R(\omega, Q_b)\right\}\ \kappa_e \tag{3}$$

where Q_a, Q_b apply to the upper and lower mantle, respectively, and

$$R(\omega, Q) = \left[\cot\left(\frac{\alpha\pi}{2}\right)\left\{1 - \left(\frac{\omega_m}{\omega}\right)^{\alpha}\right\} + i\left(\frac{\omega_m}{\omega}\right)^{\alpha}\right]\frac{1}{Q(\omega_m)}.$$

Figure 1 displays $\kappa_a(\omega)$, as well as the elastic κ_e, across the entire long-period tidal band, and Table 1 lists values for a few of the largest constituents. The anelastic effect is seen to amount to a few percent of the elastic body tide admittance at high frequencies (i.e., at periods around 1 week), climbing to about 7% at 18.6 years. Figure 1 (dashed line) shows the phase lag of the full body tide effect, i.e., $-\arg(\kappa_e + \kappa_a)$. It varies from 0.4° to 0.7°, increasing with the tidal period.

4. Ocean Tides

A completely new suite of global solutions for the long-period, zonal tides has been computed for this work. As noted above, these efforts build on previous work with the fortnightly Mf constituent [*Ray and Egbert*,

Table 1. Body Tide Contributions to Δ LOD (Major Constituents Only)

		Elastic		Anelastic		
Tide	ω (°/h)	$\Delta\Lambda$ (μs)	κ_e	$\Delta\Lambda_{\cos}$ (μs)	$\Delta\Lambda_{\sin}$ (μs)	κ_a
Node	0.0022	126.52	0.2639	8.94	1.63	0.0186 −0.0034 *i*
Sa	0.0411	22.30	0.2639	1.11	0.22	0.0131 −0.0026 *i*
Ssa	0.0821	140.38	0.2639	6.38	1.31	0.0120 −0.0025 *i*
Sta	0.1232	8.20	0.2639	0.35	0.07	0.0114 −0.0024 *i*
MSm	0.4715	30.48	0.2639	1.10	0.24	0.0095 −0.0021 *i*
Mm	0.5444	159.39	0.2639	5.61	1.25	0.0093 −0.0021 *i*
MSf	1.0159	26.44	0.2639	0.85	0.20	0.0085 −0.0020 *i*
Mf	1.0980	301.74	0.2639	9.61	2.23	0.0084 −0.0020 *i*
MSt	1.5695	10.97	0.2639	0.33	0.08	0.0080 −0.0019 *i*
Mt	1.6424	57.77	0.2639	1.73	0.41	0.0079 −0.0019 *i*
MSq	2.1139	9.23	0.2639	0.27	0.06	0.0076 −0.0018 *i*
Mq	2.1868	7.64	0.2639	0.22	0.05	0.0076 −0.0018 *i*
MSp	2.6583	2.23	0.2639	0.06	0.02	0.0074 −0.0018 *i*

2012], which showed that our purely numerical tidal solutions can be competitive with data assimilative solutions, at least for LOD predictions in the long-period band. For the work at hand, this is of considerable importance, since very nearly all of our 80 spectral lines in the long-period tidal band are too small to be reliably observed in standard ocean measurements, and therefore little reliable data exist—aside from Mf—to constrain model inversions. Yet these small lines still have significant contributions to LOD.

We have computed new solutions for nine long-period constituents. These are the major constituents and they are spread across the entire band. The oceanic LOD contributions from all the other 71 spectral lines in our model were then inferred from the admittances of these nine constituents. For eight of these nine constituents, the tides were computed by solving the Laplace tidal equations over the global ocean. The 18.6 years node tide was handled as a special case, as described below.

4.1. Dynamical Ocean Model

Similar to our earlier work, the ocean tides were computed by solving the hydrodynamic equations of motion for a barotropic fluid on a finite-difference grid. In the present case the grid resolution is 1/6°. The Arctic Ocean was included in the finite-difference grid by rotating the grid so that the North Pole was over Greenland; this is a critical step, since the Arctic is where the long-period astronomical potential is maximum and where generally the largest tidal amplitudes are expected.

Consider the depth-averaged, linearized equations of motion with current velocity $\mathbf{u}$, tidal elevation ζ, acceleration of gravity g, and ocean depth D:

$$\partial \mathbf{u}/\partial t + \mathbf{f} \times \mathbf{u} = g\,\nabla_h(\zeta - \zeta_E - \zeta_S) - r\mathbf{u}/D \tag{4}$$

$$\partial \zeta/\partial t = -\nabla_h \cdot D\mathbf{u}. \tag{5}$$

The Coriolis parameter $\mathbf{f}$ is taken oriented to the local vertical. The tidal forcing terms in (4) are (i) ζ_E, an "equilibrium tide" proportional to the astronomical potential Φ,

$$\zeta_E = \gamma_2 \Phi/g,$$

the constant γ_2 being a combination of Love numbers accounting for body tide effects, and (ii) ζ_S, a term accounting for the self attraction and Earth loading of the ocean tide, determined by a global integration of the ocean tide ζ with an appropriate kernel function [*Hendershott*, 1972], or equivalently in terms of spherical harmonics Y_n^m by

$$\zeta_S(\theta,\phi) = \sum_{n,m} \gamma'_n \alpha_n z_{nm} Y_n^m(\theta,\phi) \tag{6}$$

where z_{nm} and α_n are defined by

$$\zeta = \sum z_{nm} Y_n^m \quad \text{and} \quad \alpha_n = \frac{3(\rho_w/\rho_e)}{2n+1},$$

with ρ_w, ρ_e the mean densities of the ocean and solid Earth, respectively, and γ'_n a combination of load Love numbers [e.g., *Ray*, 1998].

In keeping with our recent work on the fortnightly constituent, we used a linearized frictional drag with coefficient $r = c_D f_v$ with c_D set to the canonical value 0.0025. The factor f_v is interpreted as a "frictional velocity" representing background currents about which the linearization is taken. After some experimentation we set f_v to a fixed 3 cm s^{-1} for all constituents.

The linearization of dissipation allows equations (4)–(5) to be solved by direct frequency-domain matrix factorization [*Egbert and Erofeeva*, 2002]. For Mf such an approach was found to be nearly as accurate (in terms of LOD effects) as a time-stepping solution of these equations, including those with nonlinear interaction terms involving short period constituents O_1 and K_1 [*Ray and Egbert*, 2012]. Iteration is necessary to account for the self-attraction/loading interaction since ζ must be known to compute ζ_S; five iterations were used in all cases.

A final point on solving equations (4) and (5) concerns the 1/6° bathymetry, which was built primarily from the General Bathymetric Chart of the Oceans 1′ grid, version 2003, with some additional refinements around

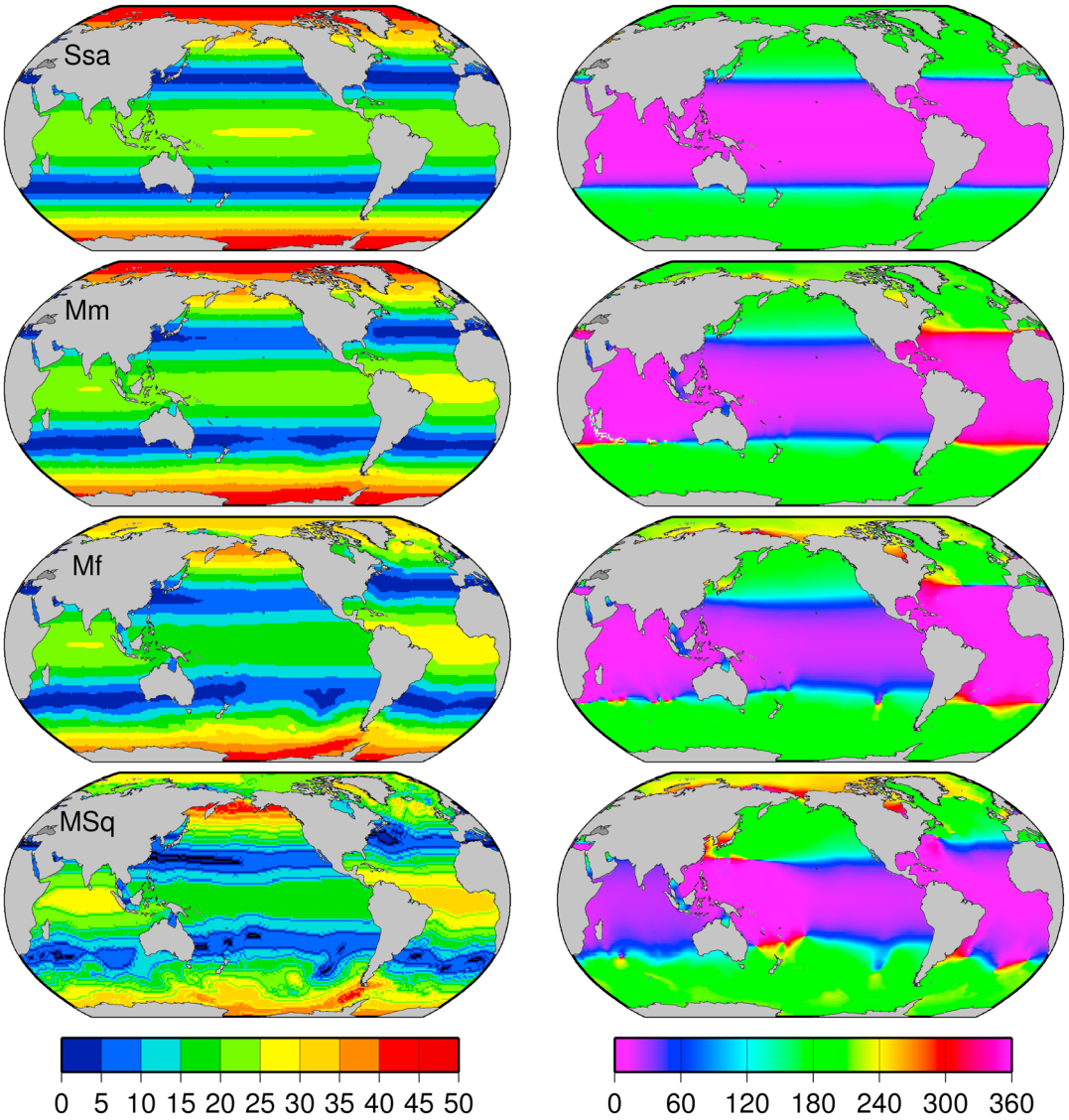

Figure 2. Cotidal charts of selected long-period zonal ocean tides (top to bottom) Ssa, Mm, Mf, and MSq, with approximate periods of semi-annual, monthly, fortnightly, and weekly. (left column) Amplitudes are in terms of tidal admittances in percentage units; to convert to elevations these should be scaled by equilibrium amplitudes V_0/g (for example, for Mf, scale by 0.0666 cm). (right column) Greenwich phase lags in degrees. As the tidal periods decrease, the ocean response becomes more dynamic and departs from a pure zonal structure.

the Antarctic continent. In regions of rough topography the bathymetry grid was slightly smoothed for the longer-period constituents Sa, Ssa, and Sta.

Figure 2 shows four of these dynamical tidal solutions, with periods of 1/2 year, 1 month, 1 fortnight, and 1 week. The amplitudes (left panels) are shown in terms of elevation admittances (relative to a constant V_0/g, not relative to Y_2^0), which allows for easy comparison of dynamical effects among the constituents. To convert these admittances to real elevations, simply scale by V_0/g. For example, along the equator the amplitudes are roughly: 8, 8, 15, and 0.5 mm for these four constituents. The extremely small amplitude of the 1 week MSq tide emphasizes why it is hopeless to attempt standard data assimilation of ocean measurements for most of these constituents; only globally integrated quantities like angular momentum are likely to be sensitive to these waves.

The maps of Figure 2 show the well-known zonal properties of the long-period tides, with the longest period displaying a near-perfect zonal structure. As the tidal period grows shorter the ocean response becomes more clearly dynamic and the zonal symmetry is broken. Differences between ocean basins in low latitudes

Table 2. Ocean Tide Contributions to Δ LOD (Major Constituents Only)

		Tidal Heights		Tidal Currents		Total		
Tide	ω (°/h)	Amp. (μs)	Phase	Amp. (μs)	Phase	Amp. (μs)	Phase	κ_o
Node	0.0022	24.39	0.0°	0.00	0.0°	24.39	0.0°	0.0509 −0.0000 *i*
Sa	0.0411	4.25	1.8°	0.01	2.9°	4.27	1.8°	0.0505 −0.0016 *i*
Ssa	0.0821	26.63	2.4°	0.12	29.6°	26.73	2.5°	0.0502 −0.0022 *i*
Sta	0.1232	1.55	3.2°	0.01	40.9°	1.56	3.4°	0.0500 −0.0029 *i*
Mm	0.5444	28.71	11.0°	1.13	63.4°	29.41	12.7°	0.0475 −0.0107 *i*
Mf	1.0980	49.15	17.3°	5.88	85.9°	51.58	23.4°	0.0414 −0.0179 *i*
Mt	1.6424	8.49	20.4°	1.75	105.1°	8.83	31.8°	0.0343 −0.0213 *i*
Mq	2.1868	1.04	22.4°	0.28	119.4°	1.04	37.7°	0.0284 −0.0219 *i*
MSp	2.6583	0.29	23.0°	0.09	127.2°	0.28	40.6°	0.0249 −0.0213 *i*

are most noticeable. For Mf the low-latitude Pacific amplitudes become considerably weaker than Atlantic amplitudes and lag them by roughly 30°. These features in Mf are very robust and have been detected in satellite altimetry and even in very schematic, flat-bottom ocean models [*Egbert and Ray*, 2003]. The reduced Mf amplitudes relative to equilibrium are also very evident in Pacific Ocean tide gauges [*Luther*, 1980].

The dynamic response in the Arctic is also remarkable. The near-maximum amplitudes seen in Ssa and Mm are seen to decay rapidly in Mf and become very small in MSq. This sharp nonequilibrium response in the high-latitude Mf was suggested even in older Geosat altimetry results [*Ray and Cartwright*, 1994], and it is clearly seen in Russian Arctic tide gauges, where phase lags increase west to east and amplitudes are well below equilibrium everywhere [*Voinov*, 2007].

4.2. Node Tide

The very long period of the node tide merits special handling. There is every reason to expect the oceanic node tide to be in near-perfect equilibrium with the tidal forcing [e.g., *Proudman*, 1960], and we have therefore computed a self-consistent—in the sense of *Agnew and Farrell* [1978]—equilibrium solution, using the same 1/6° global ocean grid used for the other constituents. Our approach uses an explicitly iterative computation, similar to that of Agnew and Farrell, but formulated in terms of spherical harmonic functions, following *Dahlen* [1976] although with a much higher degree expansion (maximum degree and order 1080). If the desired elevation admittance $\Xi(\theta, \lambda)$ is expressed

$$\Xi(\theta, \lambda) = \sum_{n,m} \xi_{nm} Y_n^m(\theta, \lambda),$$

then Ξ can be found by solving the following equation [*Dahlen*, 1976]:

$$\Xi(\theta, \lambda) = \mathcal{O}(\theta, \lambda) \left\{ \gamma_2 Y_2^0(\theta, \lambda) + \sum_{l,m} \alpha_l \gamma_l' \xi_{lm} Y_l^m(\theta, \lambda) + c \right\} \tag{7}$$

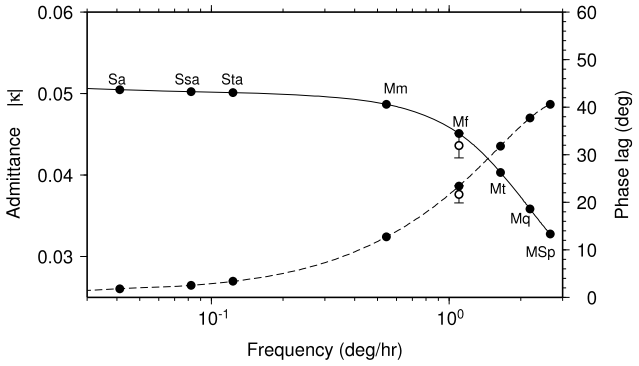

Figure 3. Magnitude (solid line) and phase lag (dashed line) of the ocean tide LOD admittance κ_o. The solid circles mark the admittances as computed from our numerical hydrodynamic tide model; a spline under tension is used to interpolate these results across all frequencies. The open circle with error bar is from a recent Mf inverse model [*Ray and Egbert*, 2012].

where $\mathcal{O}(\theta, \lambda)$ is the Munk-MacDonald ocean function and *c* is a constant introduced to ensure mass conservation, i.e., to ensure that the mean of Ξ over the global ocean is zero. The iterative solution of (7) converges rapidly; we used seven iterations, but three or four would appear to suffice. For the node tide we set the phase of Ξ, as well as the associated currents, to be identically zero.

4.3. Ocean LOD Effects

The calculation of tidal angular momenta from the tidal elevations and current velocities follow from standard integral formulas [e.g., *Chao and Ray*, 1997], and

Table 3. Long-Period Tidal Earth Rotation Rate Coefficients

	Doodson Argument							Period	V_0/g	UT(cos)	UT(sin)	$\Delta\Lambda$(cos)	$\Delta\Lambda$(sin)		
	τ	s	h	p	N'	p_s	$\pi/2$	(d)	(cm)	(μs)	(μs)	(μs)	(μs)	Re κ	Im κ
	0	0	0	0	1	−2	0	6810.443	0.00011	0.07	−7.03	0.006	0.000	0.3334	−0.0034
	0	0	0	0	1	0	2	6798.405	2.79288	1764.00	−172958.94	159.851	1.630	0.3334	−0.0034
	0	0	0	0	2	0	0	3399.202	0.02726	8.46	−840.24	1.553	0.016	0.3319	−0.0033
	0	0	0	1	0	−1	0	3232.828	0.00014	0.04	−4.22	0.008	0.000	0.3318	−0.0033
	0	0	0	2	1	0	2	1305.483	0.00379	0.47	−44.55	0.214	0.002	0.3300	−0.0035
	0	0	0	2	2	0	2	1095.178	0.00145	0.15	−14.35	0.082	0.001	0.3296	−0.0035
	0	0	1	−1	0	0	2	411.785	0.00098	0.05	−3.62	0.055	0.001	0.3277	−0.0041
	0	0	1	0	−1	−1	0	385.998	0.00420	0.19	−14.53	0.236	0.003	0.3275	−0.0042
Sa	0	0	1	0	0	−1	0	365.259	0.49215	20.78	−1608.33	27.666	0.358	0.3274	−0.0042
	0	0	1	0	0	1	2	365.225	0.02583	1.09	−84.40	1.452	0.019	0.3274	−0.0042
	0	0	1	0	1	−1	2	346.636	0.00311	0.13	−9.64	0.175	0.002	0.3273	−0.0043
	0	0	1	0	1	1	0	346.604	0.00153	0.06	−4.74	0.086	0.001	0.3273	−0.0043
	0	0	2	−2	−1	0	2	212.323	0.00205	0.05	−3.88	0.115	0.002	0.3263	−0.0045
	0	0	2	−2	0	0	0	205.892	0.03121	0.80	−57.28	1.748	0.024	0.3263	−0.0046
	0	0	2	−2	1	0	2	199.840	0.00289	0.07	−5.15	0.162	0.002	0.3262	−0.0046
	0	0	2	0	0	−2	0	182.630	0.01202	0.28	−19.55	0.673	0.010	0.3261	−0.0047
Ssa	0	0	2	0	0	0	0	182.621	3.09884	71.94	−5042.06	173.475	2.475	0.3261	−0.0047
	0	0	2	0	1	0	2	177.844	0.07719	1.76	−122.29	4.321	0.062	0.3260	−0.0047
	0	0	2	0	2	0	2	173.310	0.01702	0.38	−26.27	0.952	0.014	0.3260	−0.0047
Sta	0	0	3	0	0	−1	0	121.749	0.18092	3.20	−195.78	10.104	0.165	0.3253	−0.0053
	0	0	3	0	1	−1	2	119.607	0.00318	0.06	−3.38	0.178	0.003	0.3252	−0.0054
	0	0	4	0	0	−2	0	91.313	0.00734	0.11	−5.95	0.409	0.008	0.3247	−0.0060
	0	1	−3	1	0	1	0	34.847	0.02877	0.30	−8.82	1.590	0.054	0.3218	−0.0109
	0	1	−2	−1	−1	0	2	32.606	0.00654	0.07	−1.87	0.361	0.013	0.3216	−0.0114
	0	1	−2	1	−1	0	2	31.962	0.04832	0.49	−13.56	2.667	0.096	0.3215	−0.0116
MSm	0	1	−2	1	0	0	0	31.812	0.67279	6.78	−187.98	37.128	1.339	0.3214	−0.0116
	0	1	−2	1	1	0	2	31.664	0.04368	0.44	−12.15	2.410	0.087	0.3214	−0.0116
	0	1	−1	−1	0	1	0	29.803	0.02162	0.21	−5.65	1.192	0.045	0.3211	−0.0121
	0	1	−1	0	0	0	2	29.531	0.01860	0.18	−4.82	1.025	0.039	0.3210	−0.0122
	0	1	0	−1	−1	0	2	27.667	0.23096	2.23	−55.99	12.716	0.506	0.3207	−0.0128
Mm	0	1	0	−1	0	0	0	27.555	3.51840	33.91	−849.42	193.690	7.731	0.3206	−0.0128
	0	1	0	−1	1	0	2	27.443	0.22833	2.20	−54.90	12.569	0.503	0.3206	−0.0128
	0	1	0	1	0	0	2	27.093	0.18829	1.80	−44.68	10.362	0.419	0.3205	−0.0129
	0	1	0	1	1	0	2	26.985	0.07660	0.73	−18.10	4.215	0.171	0.3205	−0.0130
	0	1	0	1	2	0	2	26.878	0.02057	0.20	−4.84	1.132	0.046	0.3205	−0.0130
	0	1	1	−1	0	−1	2	25.622	0.01803	0.17	−4.04	0.991	0.042	0.3202	−0.0134
	0	1	2	−1	0	0	2	23.942	0.04912	0.45	−10.27	2.696	0.119	0.3197	−0.0141
	0	1	2	−1	1	0	2	23.858	0.02445	0.22	−5.10	1.342	0.059	0.3197	−0.0141
	0	2	−4	2	0	0	0	15.906	0.01097	0.09	−1.51	0.595	0.034	0.3158	−0.0183
	0	2	−3	0	0	1	0	15.387	0.03842	0.30	−5.09	2.080	0.123	0.3154	−0.0186
	0	2	−2	0	−1	0	0	14.797	0.04163	0.32	−5.30	2.250	0.136	0.3148	−0.0190
MSf	0	2	−2	0	0	0	0	14.765	0.58366	4.48	−74.13	31.545	1.908	0.3148	−0.0190
	0	2	−2	0	1	0	2	14.733	0.03740	0.29	−4.74	2.021	0.122	0.3148	−0.0191
	0	2	−1	0	0	1	0	14.192	0.02016	0.15	−2.46	1.088	0.067	0.3142	−0.0195
	0	2	0	−2	−1	0	2	13.805	0.01535	0.11	−1.82	0.827	0.052	0.3138	−0.0197
	0	2	0	−2	0	0	0	13.777	0.28836	2.15	−34.07	15.536	0.978	0.3138	−0.0198
	0	2	0	−2	1	0	2	13.749	0.01871	0.14	−2.21	1.008	0.064	0.3138	−0.0198
Mf	0	2	0	0	0	0	0	13.661	6.66068	49.36	−779.88	358.699	22.702	0.3137	−0.0199
	0	2	0	0	1	0	0	13.633	2.76162	20.45	−322.67	148.708	9.423	0.3136	−0.0199
	0	2	0	0	2	0	0	13.606	0.25828	1.91	−30.11	13.907	0.882	0.3136	−0.0199
	0	2	1	0	0	−1	2	13.168	0.02290	0.17	−2.58	1.231	0.079	0.3131	−0.0202
	0	2	2	−2	0	0	2	12.811	0.02001	0.14	−2.19	1.074	0.070	0.3126	−0.0205
	0	2	2	−2	1	0	2	12.787	0.00770	0.06	−0.84	0.414	0.027	0.3126	−0.0205
	0	3	−4	1	0	0	0	10.085	0.01794	0.111	−1.524	0.949	0.069	0.3082	−0.0225
	0	3	−3	1	0	1	0	9.814	0.01118	0.068	−0.922	0.590	0.044	0.3076	−0.0227
	0	3	−2	−1	−1	0	0	9.627	0.00947	0.057	−0.765	0.500	0.037	0.3072	−0.0228
	0	3	−2	−1	0	0	0	9.614	0.09251	0.555	−7.464	4.879	0.363	0.3072	−0.0228
MSt	0	3	−2	1	0	0	0	9.557	0.24217	1.447	−19.417	12.766	0.952	0.3070	−0.0229
	0	3	−2	1	1	0	0	9.543	0.10038	0.599	−8.036	5.291	0.395	0.3070	−0.0229
	0	3	−2	1	2	0	0	9.530	0.00907	0.054	−0.725	0.478	0.036	0.3070	−0.0229
	0	3	−1	−1	0	1	0	9.367	0.01190	0.070	−0.934	0.626	0.047	0.3066	−0.0230
	0	3	0	−3	0	0	0	9.185	0.02316	0.134	−1.780	1.218	0.092	0.3062	−0.0231
Mt	0	3	0	−1	0	0	0	9.133	1.27531	7.367	−97.403	67.010	5.068	0.3060	−0.0231
	0	3	0	−1	1	0	0	9.121	0.52856	3.050	−40.311	27.770	2.101	0.3060	−0.0232
	0	3	0	−1	2	0	0	9.108	0.04951	0.285	−3.771	2.601	0.197	0.3060	−0.0232
	0	3	1	−1	0	−1	2	8.910	0.01073	0.061	−0.798	0.563	0.043	0.3055	−0.0233
	0	4	−4	0	0	0	0	7.383	0.00897	0.043	−0.546	0.464	0.037	0.3014	−0.0238
	0	4	−3	0	0	1	0	7.236	0.01374	0.065	−0.818	0.710	0.056	0.3009	−0.0238
	0	4	−2	−2	0	0	0	7.127	0.01095	0.051	−0.641	0.565	0.045	0.3006	−0.0238

Table 3. (continued)

	Doodson Argument							Period	V_0/g	UT(cos)	UT(sin)	ΔΛ(cos)	ΔΛ(sin)		
	τ	s	h	p	N'	p_s	$\pi/2$	(d)	(cm)	(μs)	(μs)	(μs)	(μs)	Re κ	Im κ
MSq	0	4	−2	0	0	0	0	7.096	0.20369	0.940	−11.869	10.509	0.832	0.3005	−0.0238
	0	4	−2	0	1	0	0	7.088	0.08441	0.389	−4.913	4.355	0.345	0.3005	−0.0238
	0	4	−2	0	2	0	0	7.081	0.00787	0.036	−0.458	0.406	0.032	0.3005	−0.0238
Mq	0	4	0	−2	0	0	0	6.859	0.16872	0.751	−9.480	8.684	0.688	0.2998	−0.0238
	0	4	0	−2	1	0	0	6.852	0.06995	0.311	−3.926	3.600	0.285	0.2998	−0.0238
	0	5	−4	1	0	0	0	5.802	0.00950	0.035	−0.44	0.484	0.038	0.2966	−0.0233
MSp	0	5	−2	−1	0	0	0	5.643	0.04921	0.176	−2.247	2.502	0.195	0.2961	−0.0231
	0	5	−2	−1	1	0	0	5.638	0.02039	0.073	−0.930	1.037	0.081	0.2961	−0.0231
	0	5	0	−3	0	0	0	5.492	0.01898	0.066	−0.843	0.964	0.075	0.2957	−0.0230
	0	5	0	−3	1	0	0	5.488	0.00787	0.027	−0.349	0.400	0.031	0.2957	−0.0230
	0	6	−2	−2	0	0	0	4.684	0.00814	0.023	−0.307	0.412	0.031	0.2946	−0.0222

the conversion to LOD perturbations follows from *Gross* [2007, equation (46)]. Results for our nine major constituents are tabulated in Table 2. The contribution of tidal heights, which add directly to the Earth's flattening, dominates the contributions of tidal currents to the LOD, and this is magnified at longer periods as the currents become ever weaker. At shorter periods the LOD height terms lag the tidal forcing by 15°–25°, a fairly large amount, which is likely related to the clear phase lags seen in the tidal elevations in tropical oceans—see Figure 2. The LOD current terms lag by a greater amount, and are roughly in quadrature at short period.

The ocean tide's LOD admittance κ_o is shown across the entire long-period band in Figure 3. The interpolation between major constituents was done with a cubic spline under tension. The real part of the admittance is quite flat at around 0.05 across a wide-frequency band, but it starts to drop significantly around the fortnightly period and at period 1 week it is only about 0.025, or half the value at longer periods. The drop at shorter periods is a manifestation of the ocean's response becoming more dynamic and its energy scattered into modes other than the near-equilibrium Y_2^0 spherical harmonic. Correspondingly the imaginary part of κ_o also grows at shorter periods as the elevation lags grow longer and the tidal currents come more into play.

Note that the LOD effects for Mf in Table 2 do not agree exactly with the Mf inverse model used in our earlier work [*Ray and Egbert*, 2012]. The inverse model had an LOD amplitude of 49.9 μs and phase lag of 21.65°, which differs from the Table -2 values by about 3%, or roughly by the quoted standard error of the inverse solution. The inverse solution is likely more accurate, but since the two solutions differ within the standard error—see also Figure 3—we here kept the purely numerical solution to maintain consistency across all ocean tide constituents.

Comparison of Tables 1 and 2 shows that the ocean tide effect in LOD amounts to between 10% and 20% of the elastic body tide effect, a significant contribution. The anelastic part of the body tide is much smaller, several times smaller than the ocean tide, which is why efforts to determine anelasticity from observations of LOD have often been thwarted by inadequate knowledge of the ocean tide. At longer periods, however, the anelastic part dominates the phase lag in LOD, but our phase is not reliable since it is based on extrapolations from higher frequency estimates—see discussion in section 3.

5. A New LOD Model and Its Assessment

Adding the elastic body, anelastic body, and ocean tidal admittances produces the full rotation model, which is given in Table 3 for all 80 selected frequencies of the long-period tidal band.

Like *Yoder et al.* [1981], most writers on the subject of tidal LOD as well as on the subject of nutation [e.g., *Kinoshita*, 1977], express the arguments ωt in (1) as linear combinations of the fundamental variables E. W. Brown employed in his lunar theory. The tidal arguments adopted by *Woolard* [1959] are closely related. We prefer Doodson's convention instead. As is well known, Doodson, who also used Brown's lunar theory, reexpressed his final series in terms of six fundamental variables: (τ, s, h, p, N', p_s), being, respectively, mean lunar time (superfluous for long-period tides) and mean longitudes of the Moon, the Sun, the lunar perigee, the lunar node (negative), and the solar perigee. The advantage of Doodson's system stems from the very different temporal rates of the six variables, so that when tidal lines are tabulated by frequency, the integer

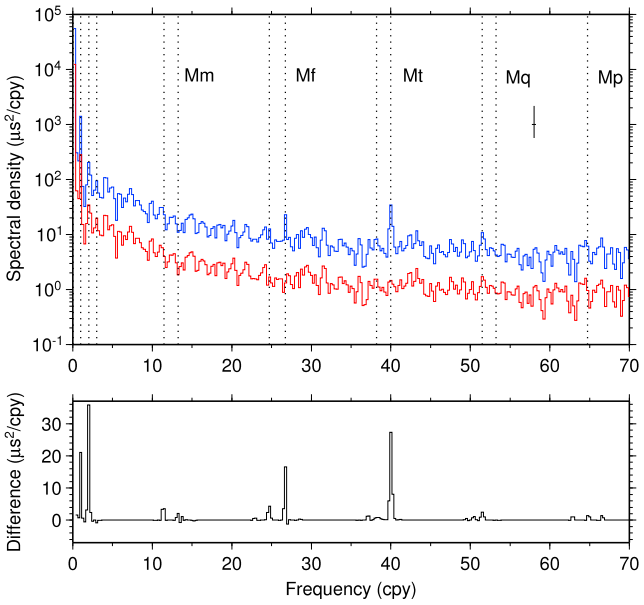

Figure 4. (top) Residual spectrum of LOD after removing all geophysical models, including tides. Blue line is based on using the long-period LOD tidal model in the 2010 IERS Conventions [*Petit and Luzum*, 2010]; red line is based on using the model presented here (curve is displaced downward for presentation purposes). LOD time series is from SPACE2008 for the period July 1989 to July 2009. Dotted lines mark frequencies of major constituents (specifically those constituents having labels in Table 3). Error bar is 95% confidence interval for both spectra. (bottom) The difference between the top two curves. Positive difference denotes that energy has been removed from the residual spectrum with our new LOD model. Largest improvements occur for tidal constituents Sa, Ssa, Mf, and Mt.

expansion coefficients fall into a simple, orderly pattern. Or as Doodson himself wrote, "it is a curious fact that if we classify in terms of τ, with a sub-classification with regard to s, and a further sub-classification with regard to h, the constituents are completely separated into groups with no over-lapping of speeds [frequencies]. It is still more curious that to the order required the same process can be continued for all the variables. Owing to this, a rather elegant and very useful form of presentation of the results is possible" [*Doodson*, 1921]. In fact, there are cases where the frequencies actually do overlap in the Hartmann-Wenzel development owing to the extremely high order of its expansion, but certainly no overlaps occur in the long-period band of our Table 3.

To the standard Doodson argument we add a seventh index, a simple multiple of 90°, which permits the cosine function to be used consistently with all arguments and ensures all amplitudes are positive. (The original expansions of Doodson and Cartwright-Tayler, and likewise Yoder et al., required both positive and negative amplitudes).

In addition to coefficients for ΔUT and $\Delta\Lambda$, Table 3 also lists the total complex admittances κ. As seen above, the imaginary part Im κ arises at the longest periods mostly from mantle anelasticity and at the shortest periods mostly from the ocean's dynamic response.

The only realistic test of this new tidal LOD model is to examine how well it removes tidal energy from real LOD measurements. To test that we use the SPACE2008 time series of Earth rotation variations produced by *Ratcliff and Gross* [2010] from various types of space-geodetic measurements. Their method employs a specially designed Kalman filter to combine disparate types of measurements and to produce a time series with daily sampling interval; see also *Gross et al.* [1998]. After computing and subtracting the new LOD tidal model from the SPACE2008 data, we examine the residual spectrum for the possible presence of peaks at known tidal frequencies.

Gross [2009] performed such tests on the current IERS tide model and also a previously adopted IERS model, as well as some others. He found the current IERS model to be mostly satisfactory although it left a clear residual peak at the period of Mt and possibly MSq. In order to highlight these small residual peaks it is necessary to remove as much nontidal energy from the LOD spectrum as possible. Gross used models of atmospheric and nontidal oceanic angular momentum based on then-standard models available from the IERS. Since then a new comprehensive and consistent model of atmospheric, oceanic, and hydrologic angular momentum has been developed by workers at the GeoForschungsZentrum (GFZ) in Potsdam [*Dobslaw et al.*, 2010]. The GFZ model is considerably better than the standard IERS model at removing nontidal variability from observed LOD in the long-period band [*Ray and Egbert*, 2012, Table 1], and it is therefore capable of better revealing residual tidal energy in the spectrum.

Figure 4 shows the LOD spectrum after correcting the SPACE2008 time series for nontidal variability with the GFZ model, and after correcting for tidal variability with (blue line) the IERS model and (red, offset curve) our new model of Table 3. Compared with the residual spectrum shown by *Gross* [2009], the

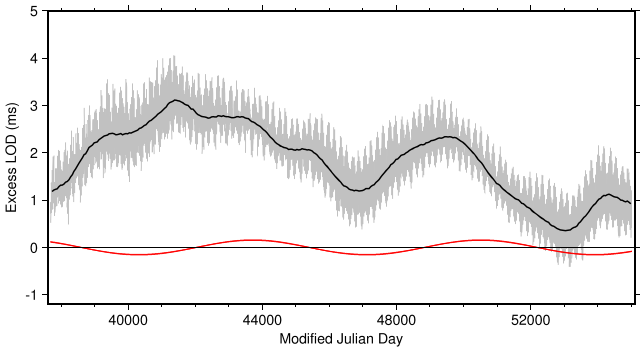

Figure 5. Excess length of day $\Delta\Lambda$ (ms) over the period January 1962 to July 2009 (modified Julian dates 37,680–55,020). Gray line is daily data extracted from the COMB2008 time series of *Ratcliff and Gross* [2010], after correction for nontidal atmospheric and oceanic angular momentum [*Dobslaw et al.*, 2010]. Black line is same data after applying yearly running mean to highlight long-period variability. Red line is the contribution to LOD from all tidal lines longer than 1 year, which is primarily the line at 18.6 years. According to Table 3, its amplitude is 0.160 ms. In the observed LOD series, the 18.6 year line is obscured by decadal variability from nontidal processes [cf. *Chao et al.*, 2014].

spectrum here, owing to the GFZ model, has much lower background energy, and it more clearly highlights residual tide problems. In the blue curve, residual peaks are now clearly evident at Mf and MSq frequencies and especially at the Mt frequency. In the red curve, these residuals are mostly removed. There may, however, be a very small residual at MSq, although it is difficult to distinguish with certainty from background.

To focus more clearly on the two spectra, Figure 4 (bottom) shows the difference, which is flat, of course, except at tidal frequencies. A positive difference implies the new LOD model is better at removing tidal energy. From that panel it is clear that considerable improvements are obtained not only at the Mf and Mt peaks, but at many others, including the solar constituents Sa and Ssa which are mostly driven by nontidal meteorological processes but which also clearly have significant tidal components which are now better modeled. It is also worth noting small positive peaks at frequencies above 50 and 60 cpy. Even though hardly above background, these peaks are all positive and therefore represent small, but real, improvements in modeling.

At the longest periods of Table 3, and most notably at 18.6 years, there appears little that observed LOD data can reveal about the reliability of our model. The amplitude of $\Delta\Lambda$ at 18.6 years is 160 μs, with a small out-of-phase component of 1.6 μs. The amplitude in the 2010 IERS model [*Petit and Luzum*, 2010, Table 8.1] is 149.5 μs. As Figure 5 makes clear, the 18.6 year tidal signal, and certainly the 10 μs difference between the two models, is buried in the observed LOD data by decadal, nontidal variability, presumably from processes in the Earth's core. As emphasized in section 3 our model at 18.6 years is based on extrapolation from much higher frequencies and is surely in some error. Unfortunately, observations of LOD are unlikely to reveal the magnitude of that error until the time series is considerably longer.

6. Summary

The new model presented here of LOD variations from long-period zonal tides offers two benefits over the model now adopted in the 2010 IERS Conventions. (1) It treats all spectral lines in the long-period band consistently—effects of mantle anelasticity and dynamic oceans are included at all frequencies. (2) It improves on the current model by successfully removing tidal variance from observed LOD time series. Considerable improvement is evident for constituents Sa, Ssa, MSm, MSf, Mf, and Mt. For most long-period constituents there are no high-quality oceanographic measurements available to test models; observed LOD data may be the only way to observe the smallest constituents, even if as global integrals, so it is satisfying to see reduced residual tidal variances. It is possible (see Figure 4) that a tiny residual peak at the frequency of MSq (period 7.1 days) leaves room for future model improvements, but the peak is hardly above background and likely requires improved models of nontidal variability to better isolate and test it.

Acknowledgments
We thank Gary Egbert, Duncan Agnew, and Shailen Desai for useful discussions and comments. This work was supported by the National Aeronautics and Space Administration's Ocean Surface Topography and Earth Surface/Interiors programs.

References

Agnew, D. C. (1981), Nonlinearity in rock: Evidence from Earth tides, *J. Geophys. Res.*, *86*, 3969–3978.
Agnew, D. C., and W. R. Farrell (1978), Self-consistent equilibrium ocean tides, *Geophys. J. R. Astron. Soc.*, *55*, 171–182.
Benjamin, D., J. Wahr, R. D. Ray, G. D. Egbert, and S. D. Desai (2006), Constraints on mantle anelasticity from geodetic observations, and implications for the J_2 anomaly, *Geophys. J. Int.*, *165*, 3–16, doi:10.1111/j.1365-246X.2006.02915.x.
Cartwright, D. E., and R. J. Tayler (1971), New computations of the tide-generating potential, *Geophys. J. R. Astron. Soc.*, *23*, 45–74.
Chao, B. F., and R. D. Ray (1997), Oceanic tidal angular momentum and Earth's rotation variations, *Prog. Oceanogr.*, *40*, 399–421.

Chao, B. F., W. Chung, Z. Shih, and Y. Hsieh (2014), Earth's rotation variations: A wavelet analysis, *Terra Nova*, doi:10.1111/ter.12094, in press.
Cheng, M. K., B. D. Tapley, and J. C. Ries (2013), Deceleration in the Earth's oblateness, *J. Geophys. Res. Solid Earth*, *118*, 740–747, doi:10.1002/jgrb.50058.
Dahlen, F. A. (1976), The passive influence of the oceans upon the rotation of the Earth, *Geophys. J. R. Astron. Soc.*, *46*, 363–406.
Defraigne, P., and I. Smits (1999), Length of day variations due to zonal tides for an inelastc Earth in non-hydrostatic equilibrium, *Geophys. J. Int.*, *139*, 563–572.
Dobslaw, H., R. Dill, A. Grötzsch, A. Brzeziński, and M. Thomas (2010), Seasonal polar motion excitation from numerical models of atmosphere, ocean, and continental hydrosphere, *J. Geophys. Res.*, *115*, B10406, doi:10.1029/2009JB007127.
Doodson, A. T. (1921), The harmonic development of the tide-generating potential, *Proc. R. Soc. London, Ser. A*, *100*, 305–329.
Egbert, G. D., and S. Y. Erofeeva (2002), Efficient inverse modeling of barotropic ocean tides, *J. Atmos. Oceanic Technol.*, *19*, 183–204.
Egbert, G. D., and R. D. Ray (2003), Deviation of long-period tides from equilibrium: Kinematics and geostrophy, *J. Phys. Oceanogr.*, *33*, 822–839.
Gross, R. S. (2007), Earth rotation variations: Long period, in *Treatise on Geophysics, Geodesy, chap. 9*, vol. 3, edited by G. Schubert, pp. 239–294, Elsevier, Amsterdam, Netherlands.
Gross, R. S. (2009), Ocean tidal effects on Earth rotation, *J. Geodyn.*, *48*, 219–225.
Gross, R. S., T. M. Eubanks, J. A. Steppe, A. P. Freedman, J. O. Dickey, and T. F. Runge (1998), A Kalman-filter-based approach to combining independent Earth orientation series, *J. Geod.*, *72*, 213–235.
Hartmann, T., and H.-G. Wenzel (1995), The HW95 tidal potential catalogue, *Geophys. Res. Lett.*, *22*, 3553–3556.
Hendershott, M. C. (1972), The effects of solid Earth deformation on global ocean tides, *Geophys. J. R. Astron. Soc.*, *29*, 389–402.
Kinoshita, H. (1977), Theory of rotation of the rigid Earth, *Celestial Mech.*, *15*, 277–326.
Kudryavtsev, S. M. (2004), Improved harmonic development of the Earth tide-generating potential, *J. Geod.*, *77*, 829–838.
Lambeck, K. (1980), *The Earth's Variable Rotation: Geophysical Causes and Consequences*, Cambridge Univ. Press, Cambridge, U. K.
Lambeck, K., and S. M. Nakiboglu (1983), Long-period Love numbers and their frequency dependence due to dispersion effects, *Geophys. Res. Lett.*, *10*, 857–860.
Luther, D. S. (1980), Observations of long period waves in the tropical oceans and atmosphere, PhD thesis, MIT, Cambridge, Mass.
Mathews, P. M., V. Dehant, and J. M. Gipson (1997), Tidal station displacements, *J. Geophys. Res.*, *102*, 20,469–20,477.
Munk, W. H., and D. E. Cartwright (1966), Tidal spectroscopy and prediction, *Philos. Trans. R. Soc. London, Ser. A*, *A259*, 533–581.
Petit, G., and B. Luzum (2010), IERS Conventions 2010, *Tech. Note 36.*, International Earth rotation and reference systems service, Verlag des Bundesamts für Kartographie und Geodäsie.
Proudman, J. (1960), The condition that a long-period tide shall follow the equilibrium law, *Geophys. J. R. Astron. Soc.*, *3*, 244–249.
Ratcliff, J. T., and R. S. Gross, (2010), Combinations of Earth orientation measurements: SPACE2008, COMB2008, and POLE2008, *JPL Pub. 10-4*, Jet Propulsion Laboratory, Pasadena, Calif.
Ray, R. D. (1998), Ocean self-attraction and loading in numerical tidal models, *Mar. Geod.*, *21*, 181–192.
Ray, R. D., and D. E. Cartwright (1994), Satellite altimeter observations of the Mf and Mm ocean tides, in *Gravimetry and Space Techniques Applied to Geodynamics and Ocean Dynamics*, edited by B. E. Schutz et al., pp. 69–78, AGU, Washington, D. C.
Ray, R. D., and G. D. Egbert (2012), Fortnightly Earth rotation, ocean tides, and mantle anelasticity, *Geophys. J. Int.*, *189*, 400–413.
Roosbeek, F. (1996), RATGP95: A harmonic development of the tide-generating potential using an analytical method, *Geophys. J. Int.*, *126*, 197–204.
Sipkin, S. A., and T. H. Jordan (1980), Regional variation of Q_{ScS}, *Bull. Seismol. Soc. Am.*, *70*, 1071–1102.
Smith, M. L., and F. A. Dahlen (1981), The period and Q of the Chandler wobble, *Geophys. J. R. Astron. Soc.*, *64*, 223–282.
Voinov, G. I. (2007), Monthly and fortnightly tides in the Russian Arctic seas, *Oceanology*, *47*, 626–635.
Wahr, J. M., and Z. Bergen (1986), The effects of mantle anelasticity on nutations, Earth tides, and tidal variations in rotation rate, *Geophys. J. R. Astron. Soc.*, *87*, 633–668.
Wahr, J. M., T. Sasao, and M. L. Smith (1981), Effect of the fluid core on changes in the length of day due to long period tides, *Geophys. J. R. Astr. Soc.*, *64*, 635–650.
Woolard, E. W. (1953), Theory of rotation of the Earth about its center of mass, in *Astronomical Papers: American Ephemeris and Nautical Almanac, Part I*, vol. 15, pp. 3–165, U. S. Gov't. Printing Office, Washington, D. C.
Woolard, E. W. (1959), Inequalities in mean solar time from tidal variations in the rotation of the Earth, *Astron. J*, *64*, 140–142.
Yoder, C. F., J. G. Williams, and M. E. Parke (1981), Tidal variations of Earth rotation, *J. Geophys. Res.*, *86*, 881–891.